Therapeutic Potential of Adipose-Derived SSEA-3-Positive Muse Cells for Treating Diabetic Skin Ulcers

KAHORI KINOSHITA,[a] SHINICHIRO KUNO,[a] HISAKO ISHIMINE,[b] NORIYUKI AOI,[a] KAZUHIDE MINEDA,[a] HARUNOSUKE KATO,[a] KENTARO DOI,[a] KOJI KANAYAMA,[a] JINGWEI FENG,[a] TAKANOBU MASHIKO,[a] AKIRA KURISAKI,[b] KOTARO YOSHIMURA[a]

[a]Department of Plastic Surgery, University of Tokyo Graduate School of Medicine, Tokyo, Japan; [b]Research Center for Stem Cell Engineering, National Institute for Advanced Industrial Science and Technology, Ibaraki, Japan

Correspondence: Kotaro Yoshimura, M.D., Department of Plastic Surgery, University of Tokyo School of Medicine, 7-3-1, Hongo, Bunkyo-Ku, Tokyo 113-8655, Japan. Telephone: 81-3-5800-8948; E-Mail: kotaro-yoshimura@umin.ac.jp

ABSTRACT

Stage-specific embryonic antigen-3 (SSEA-3)-positive multipotent mesenchymal cells (multilineage differentiating stress-enduring [Muse] cells) were isolated from cultured human adipose tissue-derived stem/stromal cells (hASCs) and characterized, and their therapeutic potential for treating diabetic skin ulcers was evaluated. Cultured hASCs were separated using magnetic-activated cell sorting into positive and negative fractions, a SSEA-3+ cell-enriched fraction (Muse-rich) and the remaining fraction (Muse-poor). Muse-rich hASCs showed upregulated and downregulated pluripotency and cell proliferation genes, respectively, compared with Muse-poor hASCs. These cells also released higher amounts of certain growth factors, particularly under hypoxic conditions, compared with Muse-poor cells. Skin ulcers were generated in severe combined immunodeficiency (SCID) mice with type 1 diabetes, which showed delayed wound healing compared with nondiabetic SCID mice. Treatment with Muse-rich cells significantly accelerated wound healing compared with treatment with Muse-poor cells. Transplanted cells were integrated into the regenerated dermis as vascular endothelial cells and other cells. However, they were not detected in the surrounding intact regions. Thus, the selected population of ASCs has greater therapeutic effects to accelerate impaired wound healing associated with type 1 diabetes. These cells can be achieved in large amounts with minimal morbidity and could be a practical tool for a variety of stem cell-depleted or ischemic conditions of various organs and tissues. STEM CELLS TRANSLATIONAL MEDICINE 2015;4:146–155

INTRODUCTION

Bone marrow has been used for many years as a treatment of leukemia, and the mesenchymal stem cells (MSCs) contained in transplanted bone marrow have been shown to differentiate into tissue-specific cells in various organs [1–3]. Although previous results suggested that MSCs derived from bone marrow or skin contain a fraction of pluripotent or multipotent cells [1, 2, 4, 5], the multipotent cells were not well characterized, because they were considered very rare and lacked a specific surface marker. Kuroda et al. [6] reported a unique subset of human MSCs that can be efficiently isolated as cells double positive for mesenchymal marker CD105+ and human pluripotent stem cell marker stage specific embryonic antigen (SSEA)-3+ cells. They are also able to self-renew and differentiate into cells representative of all three germ layers, namely endodermal, ectodermal, and mesodermal cells from a single cell [6]. These cells were initially identified by applying stress to MSCs and were termed multilineage differentiating stress-enduring cells

(Muse cells). Although Muse cells do not have high proliferative activity, they were reported to generate multiple cell types of the three germ layers without inducing unfavorable tumors [6]. Thus, Muse cells appear to be safer than other induced pluripotent or multipotent cells and might have better therapeutic potential than general (non-Muse) MSCs. Although Muse cells were not identified in animals other than a goat [7], they have been sparsely detected around vessels in various human mesodermal organs or tissues such as the skin and subcutis [8–10]. Muse cells were also reported to home to injured regions and spontaneously differentiate into tissue-specific functional cells in the damaged liver, skin, and skeletal muscle in animal models [6].

In the present report, we isolated SSEA-3+ Muse cells from patient-derived human adipose tissue-derived stem/stromal cells (hASCs). We characterized the adipose-derived Muse cells and evaluated their therapeutic potential in treating diabetic refractory skin ulcers. Skin ulcers under ischemic conditions generally show
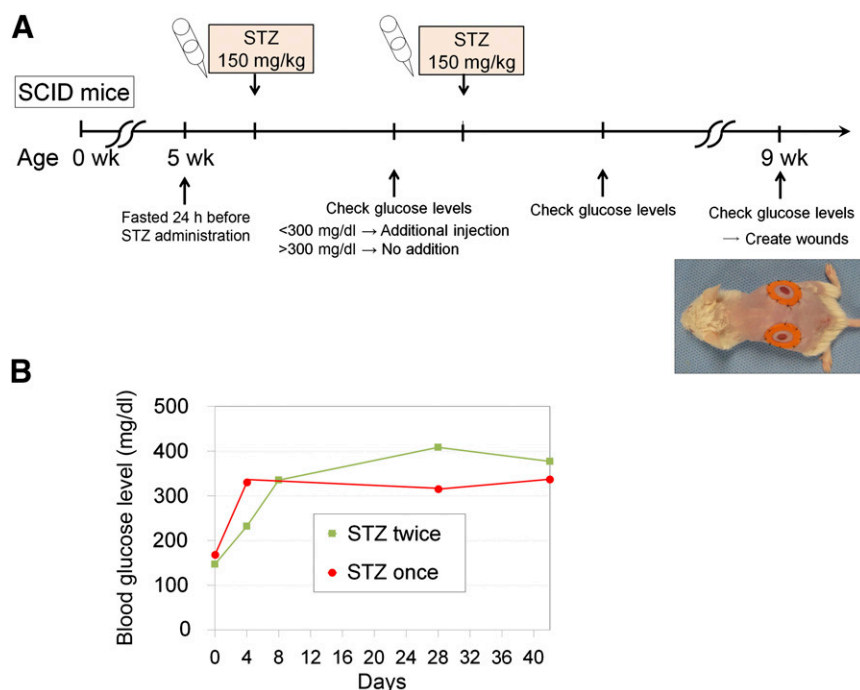
Figure 1. Preparation of immunodeficient diabetic mice. **(A):** We prepared immunodeficient mice with diabetes mellitus (DM) for a wound healing experiment. To induce type 1 DM, STZ was injected intraperitoneally into 5-week-old male SCID mice that had been fasted for 24 hours. Three days after STZ (150 mg/kg) administration, hyperglycemia (blood glucose >300 mg/dl) was examined. When hyperglycemia was not observed, another STZ (150 mg/kg) injection was given. Skin defects were created on the back of DM-induced SCID mice at 9 weeks of age. **(B):** Typical changes in blood glucose level are shown. Hyperglycemia was achieved after one or two STZ injections at approximately 75%. Abbreviations: SCID, severe combined immunodeficiency; STZ, streptozotocin.

delayed wound healing and are typical therapeutic targets of cell-based therapies using MSCs or endothelial progenitor cells. In order to investigate whether Muse cells are superior to other MSCs, we compared the wound healing of skin defects in diabetic mice between treatments with the two distinct cell populations.

MATERIALS AND METHODS

Human Tissue Sampling and Cell Isolation

Liposuction aspirates were obtained from liposuction surgery from the abdomen and/or thighs after informed consent from 5 nonobese female patients (age 26.6 ± 8.7 years, body mass index 21.5 ± 2.0 kg/m^2). The ethical committee of the University of Tokyo School of Medicine approved the present study. The stromal vascular fraction (SVF) containing adipose-derived stem/stromal cells (ASCs) was isolated from the aspirated fat, as described previously [11]. In brief, aspirated fat tissue was washed with phosphate-buffered saline (PBS) and digested in PBS containing 0.075% collagenase for 30 minutes in a shaker at 37°C. Mature adipocytes and connective tissue were separated from pellets by centrifugation. The cell pellets were resuspended, filtered through 100-μm, 70-μm, and 40-μm mesh, and hemolyzed.

Cell pellets (equivalent to SVF) containing ASCs were cultured in dishes containing Dulbecco's modified Eagle's medium (DMEM) supplemented with 10% fetal bovine serum. After approximately 2 weeks in culture, expanded hASCs were subcultured in the same media. Second-passage cultured hASCs were harvested with 0.25% trypsin containing

2 mM EDTA for 5 minutes at 37°C and used for Muse cell isolation.

Muse Cell Separation

Magnetic-activated cell sorting (MACS) (autoMACS; Miltenyi Biotec, Bergisch Gladbach, Germany, http://www.miltenyibiotec.com) was used to collect SSEA-3$^+$ Muse cells. Although Muse cells are reported to be double positive for SSEA-3 and CD105, previous studies collected Muse cells using single SSEA-3 labeling because nearly 100% of mesenchymal cells, including ASCs, will be CD105$^+$ [6, 10, 12]. We, therefore, collected Muse cells using the anti-SSEA-3 antibody conjugated with phycoerythrin (PE) (dilution 1:3, Miltenyi Biotec) and anti-PE microbeads (dilution 1:2, Miltenyi Biotec) were used for MACS separation of the Muse cells. Target cell-labeled microbeads were trapped in a magnetic field and later collected as a positive fraction. The cell solution that did not attach to the magnetic column was collected as the negative fraction. To better purify a small number of Muse cells, we used a MACS program that applied the cell solution twice to the magnetic column at a very slow speed. The obtained positive cell fraction was considered the "Muse-rich" population, and the negative counterpart was considered the "Muse-poor" population.

Flow Cytometry Analyses

Flow cytometry analyses were performed before and after separation of the Muse cells using a flow cytometer (MACSQuant; Miltenyi Biotec). The SSEA-3 antibody conjugated with PE (dilution 1:3; Miltenyi Biotec) was used for the analyses.
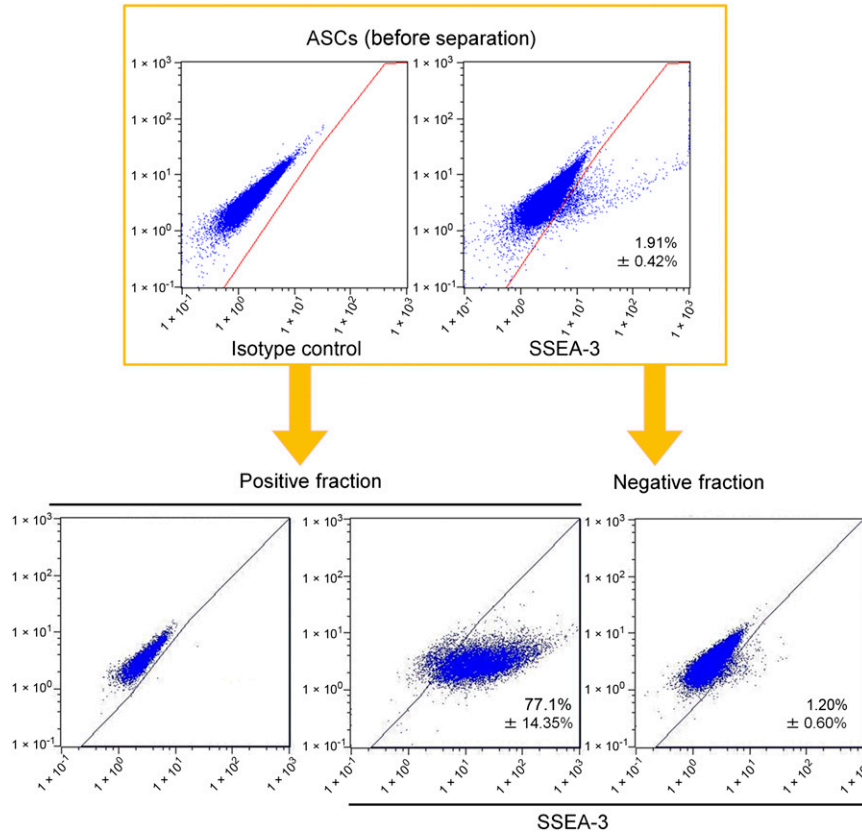
Figure 2. Flow cytometry analyses for SSEA-3 expression before and after enrichment of Muse cells using magnetic-activated cell sorting (MACS). An example of flow cytometry analysis performed to measure SSEA-3$^+$ cells before and after MACS cell enrichment and separation is shown. Cultured human ASCs were processed using MACS separation to obtain SSEA-3$^+$ cells. The positive and negative cell fractions after MACS separation were used as Muse-rich and Muse-poor cell populations, respectively, in subsequent experiments. Abbreviations: ASCs, adipose tissue-derived stem/stromal cells; SSEA-3, stage-specific embryonic antigen-3.

Cytokine Production Assays (Enzyme-Linked Immunosorbent Assays)

Muse-rich and Muse-poor cell populations were seeded at 4.0×10^5 cells in 60-mm dishes and cultured in DMEM without serum under hypoxic (1% O_2) or normoxic (6% O_2) conditions. After 48 hours, the culture media were collected and filtered using a 0.22-μm filter (Millex-GV filter; EMD Millipore, Billerica, MA, http://www.emdmillipore.com). Enzyme-linked immunosorbent assays (ELISA) kits for hepatocyte growth factor (HGF), stromal cell-derived factor 1 (SDF-1) (both from R&D Systems, Minneapolis, MN, http://www.rndsystems.com), and a cytokine array kit for vascular endothelial growth factor (VEGF), epidermal growth factor (EGF), platelet-derived growth factor (PDGF)-BB, nerve growth factor-β (NGF-β), stem cell factor (SCF), tumor necrosis factor-α (TNF-α), basic fibroblast growth factor (bFGF), and transforming growth factor-β (TGF-β) (catalog no. EA-1101; Signosis, Inc., Santa Clara, CA, http://www.signosisinc.com) were used to detect the cytokines. The absorbance was spectrophotometrically measured at 450 nm using an infinite microplate reader (M1000; Tecan Group, Männedorf, Switzerland, http://www.tecan.com).

Microarray Analyses

The samples were prepared as follows. Cultured hASCs were harvested with 0.25% trypsin and 2 mM EDTA for 5 minutes at 37°C.

Portions of the cell suspensions were collected and dissolved with Isogen (Nippon Gene, Tokyo, Japan, http://www.nippongene.com) as a control sample, and other portions were used for sorting with autoMACS. After sorting, cell suspensions of Muse-rich populations and Muse-poor populations were dissolved with Isogen as a Muse-rich sample and a Muse-poor sample, respectively. Total RNA was purified using the RNeasy mini kit (Qiagen, Hilden, Germany, http://www.qiagen.com) according to the manufacturer's recommendations. Fluorescent-labeled cRNA was synthesized using a Quick Amp Labeling Kit (Agilent Technologies, Santa Clara, CA, http://www.agilent.com). Labeled cRNAs were hybridized with the SurePrint G3 Human GE microarray $8 \times 60K$ (G4851A; Agilent Technologies). Microarrays were scanned using a G2505C microarray scanner, and the results were analyzed using Feature Extraction Software (Agilent Technologies). Finally, we analyzed gene expression using GeneSpring GX software, version 12.5 (Agilent Technologies).

Preparation of Immunodeficient Diabetic Mice

Five-week old male severe combined immunodeficient (SCID) mice (C.B-17/Icr-*scid/scid*Jcl) were purchased from CLEA Japan, Inc. (Tokyo, Japan, http://clea-japan.com). All animal experiments were performed with approval from the Institutional Animal Care and Use Committee of the University of Tokyo. After the SCID mice were fasted for 24 hours, freshly prepared
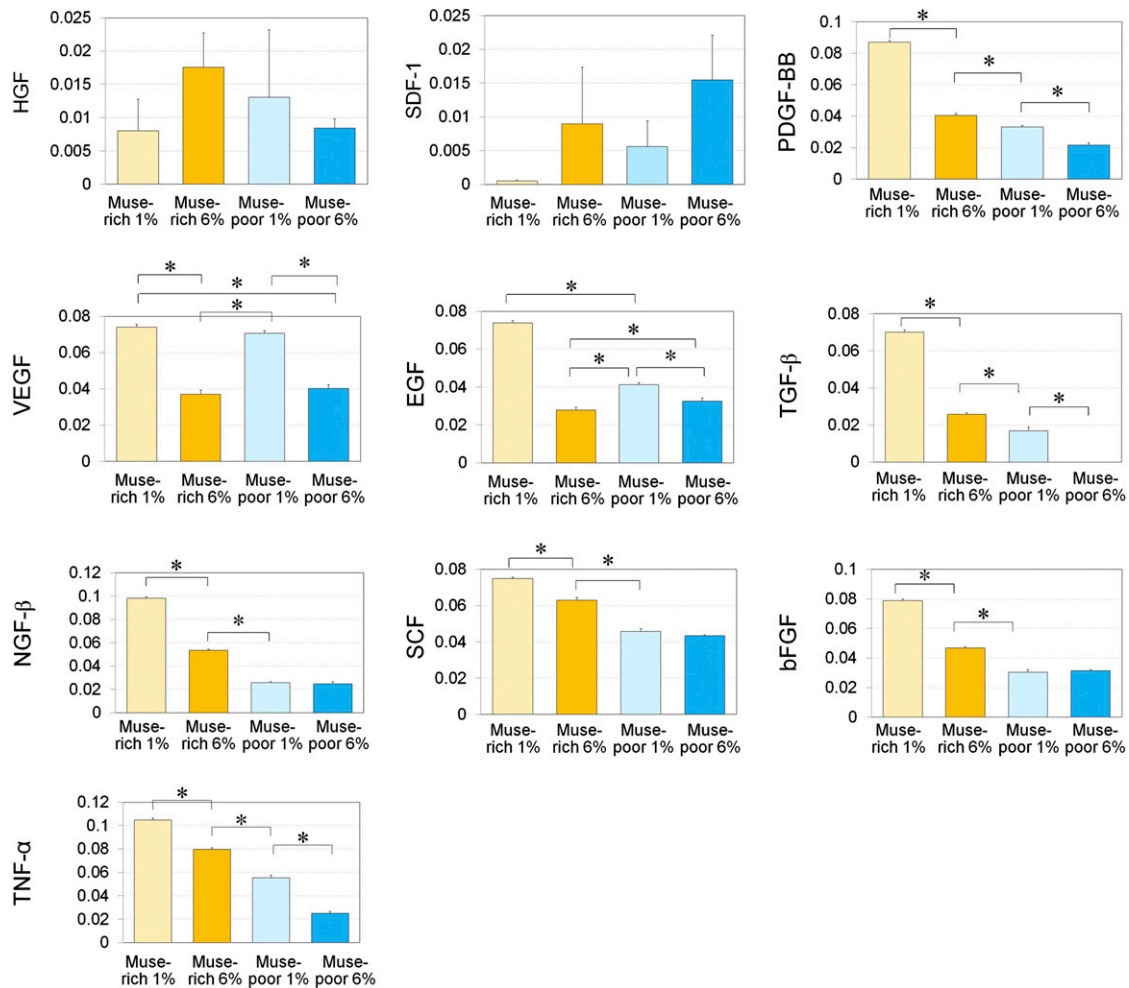
Figure 3. Enzyme-linked immunosorbent assay (ELISA) analyses for growth factor production under hypoxic and normoxic conditions. The relative growth factor production values were measured with ELISA in Muse-rich and Muse-poor cell fractions cultured under hypoxic (1% O_2) or normoxic (6% O_2) conditions for 48 hours. The measured growth factors included HGF, SDF-1, PDGF-BB, VEGF, EGF, TGF-β, NGF-β, SCF, bFGF, and TNF-α. The y-axis indicates absorbance at 450 nm. The samples were collected from three independent experiments, and three replicates were used in each measurement. Data are presented as the mean ± SD ($n = 3$). ∗, $p < .05$. Abbreviations: bFGF, basic fibroblast growth factor; EGF, epidermal growth factor; HGF, hepatocyte growth factor; Muse, multilineage-differentiating stress-enduring; NGF-β, nerve growth factor-β; PDGF-BB, platelet-derived growth factor-BB; SCF, stem cell factor; SDF-1, stromal cell-derived factor 1; TGF-β, transforming growth factor-β; TNF-α, tumor necrosis factor-α; VEGF, vascular endothelial growth factor.

streptozotocin (STZ; 150 mg/kg; Sigma-Aldrich, St. Louis, MO, http://www.http://www.sigmaaldrich.com) in citrate-saline buffer (pH 4.5) was injected intraperitoneally. The blood glucose levels were measured using a glucometer and test strips (Glucose Pilot; Aventir Biotech LLC, Carlsbad, CA, http://www.aventirbio. com) 3 days after STZ injection. When the blood glucose levels were greater than 300 mg/dl, the mice were considered to have diabetes mellitus (DM). The mice that did not show hyperglycemia (>300 mg/dl) received a second injection of STZ (150 mg/kg), and the blood glucose levels were monitored 3 days later (Fig. 1A).

Wound Healing Mice Models

To evaluate skin wound healing, skin defects were created on the back of the mice, as previously described [13, 14]. In brief, the mice were individually anesthetized via an intraperitoneal injection of pentobarbital (65 mg/kg). After removing the hair using an electric trimmer and depilatory cream, two full-thickness skin wounds (6 mm in diameter), extending through the panniculus carnosus layer, were made on the dorsum of mice using a sterile circular biopsy punch (Kai Industries Co., Tokyo, Japan, http://www.kai-group.com/global/en/). To avoid wound contraction, a donut-shaped silicon splint (internal and external diameter of 9 and 15 mm, respectively; 1.0-mm-thick silicone rubber sheet; Kyowa Industries, Saitama, Japan, http://www.kyowakg.com) was applied and fixed using a 6-0 nylon suture to avoid wound contraction (Fig. 1A). Occlusive dressing (Perme-roll; Nitto Medical, Osaka, Japan, http://www.nitto.com/jp/en/) was used to prevent wound drying and scab formation.

We prepared five experimental groups: wild-type mice (C.B-17/lcr), non-DM SCID mice (C.B-17/lcr-*scid/scid*Jcl), DM-induced SCID mice, DM-induced SCID mice treated with a Muse-rich cell population, and DM-induced SCID mice treated with a Muse-poor cell population. Six mice were used in each group. After mixing with 0.1 ml of cross-linked hyaluronic acid (Restylane; Galderma, Watford, U.K., http://www.galderma.com), Muse-rich

or Muse-poor cells (1.0×10^5 cells per mouse) were injected into the subcutis at four points (0.025 ml at each point) around the wound. Macroscopically, we examined the interval to wound closure (the number of days until the skin defect had closed completely). The wound was sequentially photographed on days 0, 3, 7, 10, and 14 using a digital camera (IXY Digital 90; Canon, Tokyo, Japan; http://www.canon.com). The photographs were evaluated to measure the wound area using image analysis software (Photoshop CS6; Adobe Systems, San Jose, CA, http://www.adobe.com).

Histological Analyses

The mice skin samples were embedded in optimal cutting temperature compound (Sakura Finetek, Tokyo, Japan, http://www.sakura-finetek.com), frozen in liquid nitrogen, and stored at $-80°C$ until sectioning. The frozen sections (8 μm) were placed on slides, air dried at room temperature for 20 minutes, fixed in 4% paraformaldehyde (in PBS) for 1 minute, and washed for 5 minutes in PBS. The slides were stained with H&E and processed for immunohistochemistry.

Immunohistochemistry was performed as described previously [6]. To detect injected human cells in the mouse skin, the sections were treated with 0.3% hydrogen peroxide in methanol for 30 minutes to inactivate intrinsic peroxidase activity and incubated sequentially with rabbit anti-human 58K Golgi protein (dilution 1:100; Abcam, Cambridge, U.K., http://www.abcam.com) and donkey anti-rabbit IgG-horseradish peroxidase (dilution 1:500; Jackson ImmunoResearch Laboratories, Inc., West Grove, PA, http://www.jacksonimmuno.com). Expression of human 58K Golgi protein was visualized by the peroxidase reaction with 3,3′-diaminobenzidine tetrahydrochloride. For laser confocal microscopy, cryosections were incubated with the following primary antibodies: mouse anti-human mitochondria (dilution 1:100, Abcam), rabbit anti-human 58K Golgi protein, or goat anti-human platelet endothelial cell adhesion molecule-1 (PECAM-1; dilution 1:50, Santa Cruz Biotechnology, Santa Cruz, CA, http://www.scbt.com). Next, the sections were incubated with the following secondary antibodies: donkey anti-mouse IgG-Alexa 488 or rabbit anti-goat IgG-Alexa 488 (all dilutions, 1:500; Invitrogen, Carlsbad, CA, http://www.invitrogen.com). Vessels (vascular endothelial cells) were stained with Alexa Fluor 594-conjugated isolectin GS-IB$_4$ (Molecular Probes, Eugene, OR, http://probes.invitrogen.com) and nuclei with Hoechst 33342 (Dojindo Molecular Technologies Inc., Kumamoto, Japan, http://www.dojindo.com) and inspected using confocal microscopy (C1si Nikon; Nikon, Tokyo, Japan, http://www.nikon.com).

Statistical Analysis

The results are expressed as the mean $\pm$ SD. Tukey's tests and Steel-Dwass tests were applied to evaluate the differences between each group; $p < .05$ was considered statistically significant.

RESULTS

Detection and Separation of Muse Cells From Cultured hASCs

hASCs were obtained by culturing SVF obtained from lipoaspirates. Flow cytometry analyses revealed that cultured hASCs at passage 2 contained a low percentage of SSEA-3$^+$ Muse cells
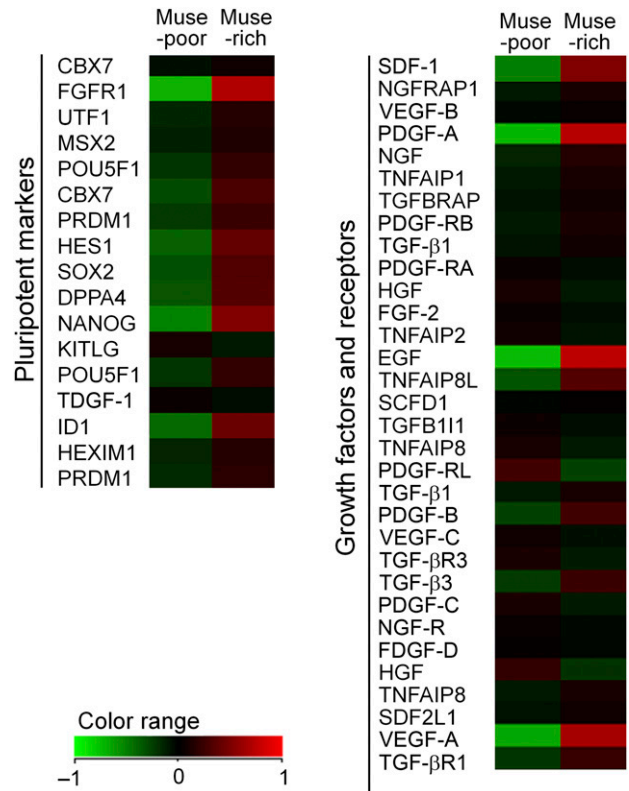

Figure 4. Microarray analyses of Muse-rich and Muse-poor cell populations. Heat maps for pluripotent markers, growth factors, and receptors indicate that pluripotent markers, including NANOG and FGFR1, were upregulated in the Muse-rich population compared with the Muse-poor population. The Muse-rich population also showed higher gene expression of growth factors such as PDGF-A, EGF, and VEGF-A (supplemental online Figure 1). Abbreviations: EGF, epidermal growth factor; FGFR1, fibroblast growth factor receptor 1; HGF, hepatocyte growth factor; Muse, multilineage-differentiating stress-enduring; NGF, nerve growth factor; PDGF-A, platelet-derived growth factor-A; SDF-1, stromal cell-derived factor 1; TGF, transforming growth factor; VEGF, vascular endothelial growth factor.

(1.91% $\pm$ 0.42%) (Fig. 2). Using MACS sorting, we collected Muse-rich and Muse-poor cell populations, both of which were used in animal wound healing experiments. In the Muse-rich population, 77.1% $\pm$ 14.35% of cells were SSEA-3$^+$. In contrast, in the Muse-poor population, 1.20% $\pm$ 0.6% of the cells were SSEA-3$^+$, suggesting that SSEA-3$^+$ ratio in Muse-poor population is very close to that in the original ASCs (Fig. 2).

Cytokine Secretion by Muse Cells Under Normoxic and Hypoxic Conditions

We compared the cytokine concentrations in culture media after 48 hours of adherent culture of Muse-rich and Muse-poor populations under normoxic (6% O$_2$) or hypoxic (1% O$_2$) conditions (Fig. 3). The Muse-rich population released greater amounts of EGF, PDGF-BB, NGF-β, SCF, TNF-α, bFGF, and TGF-β compared with the Muse-poor population cultured under the same oxygen tension (Fig. 3). In addition, the concentration of VEGF, EGF, PDGF-BB, NGF-β, SCF, TNF-α, bFGF, and TGF-β increased under hypoxic conditions compared with normoxic conditions, particularly in the Muse-rich population.

Comparative Gene Expression Profiles of Muse-Rich and Muse-Poor Cell Populations

Microarray analyses were performed to analyze differences in gene expression between the Muse-rich and Muse-poor populations (n = 1). Gene ontology analyses of the genes differentially expressed between the Muse-rich and Muse-poor populations indicated several characteristic ontologies. For example, "blood vessel morphogenesis" genes were upregulated in Muse-rich cells and "mitotic cell cycle" genes were upregulated in Muse-poor cells (supplemental online Fig. 1). We found that Muse-rich cells had upregulated expression of pluripotent markers, including NANOG and Sox2 (Fig. 4), as described previously [6]. In addition, the Muse-rich population highly expressed growth factors/cytokines such as SDF-1, PDGF-A, EGF, and VEGF-A. All microarray data obtained from our gene expression analyses were deposited with the National Center for Biotechnology Information Gene Expression Omnibus database (accession no. GSE55526).

Induction of DM in SCID Mice by STZ Injection

STZ damages the pancreatic β cells and induces type 1 DM; however, the dose and method of STZ administration have differed among previous reports [15–17]. When we administered 200 mg/kg STZ, the SCID mice frequently died of severe weight loss and metabolic abnormalities within 1 week of administration. However, injection of 150 mg/kg STZ into SCID mice after 24 hours of fasting successfully induced hyperglycemia with relative consistency, and the DM status ($>$300 mg/dl blood glucose) was maintained for longer than 30 days (Fig. 1B). DM-induced SCID mice (DM-SCID), which were successfully prepared using one (9 of 29 mice; 31.0%) or two (13 of 29 mice; 44.8%) STZ injections, were used in wound healing experiments 30 days after the final STZ injection.

Would Healing in DM-SCID Mice With or Without Cell Treatment

Compared with wild-type (WT) mice (n = 6) or non-DM-SCID mice (n = 6), wound healing was significantly delayed in the DM-SCID mice (Fig. 5). WT and non-DM-SCID mice showed wound sizes of 56.9% $\pm$ 12.0% and 67.5% $\pm$ 6.5% on day 7, respectively. In contrast, DM-SCID mice (n = 6) showed wound sizes of 95.4% $\pm$ 3.1% (WT vs. DM-SCID; $p <$ .0001). The DM-SCID mice also presented with larger wound sizes on day 14 compared with the WT or non-DM-SCID mice. Thus, the DM-SCID mice were confirmed to be an immunodeficient animal model with impaired wound healing.

The skin wounds in the DM-SCID mice were treated with a subcutaneous injection of either Muse-rich or Muse-poor cells. Muse-rich cell-treated DM-SCID mice (n = 6) showed significantly better wound healing with a statistically significant difference compared with DM-SCID mice treated with Muse-poor cells (n = 6), although the treatment using Muse-poor cells significantly accelerated wound healing compared with that of the DM-SCID mice with no treatment (Fig. 5). The wound size on day 7 was 51.05% $\pm$ 7.2% and 74.0% $\pm$ 6.6% in the DM-SCID mice treated with Muse-rich and Muse-poor cells, respectively ($p <$ .0001). The wounds had healed completely in the DM-SCID mice with Muse-rich treatment by day 14, although the wound size in the DM-SCID mice with Muse-poor treatment was 30.3% $\pm$ 6.7% (p = .0235). The wound healing in the DM-SCID mice with Muse-rich treatment on day 14 was even significantly better than that
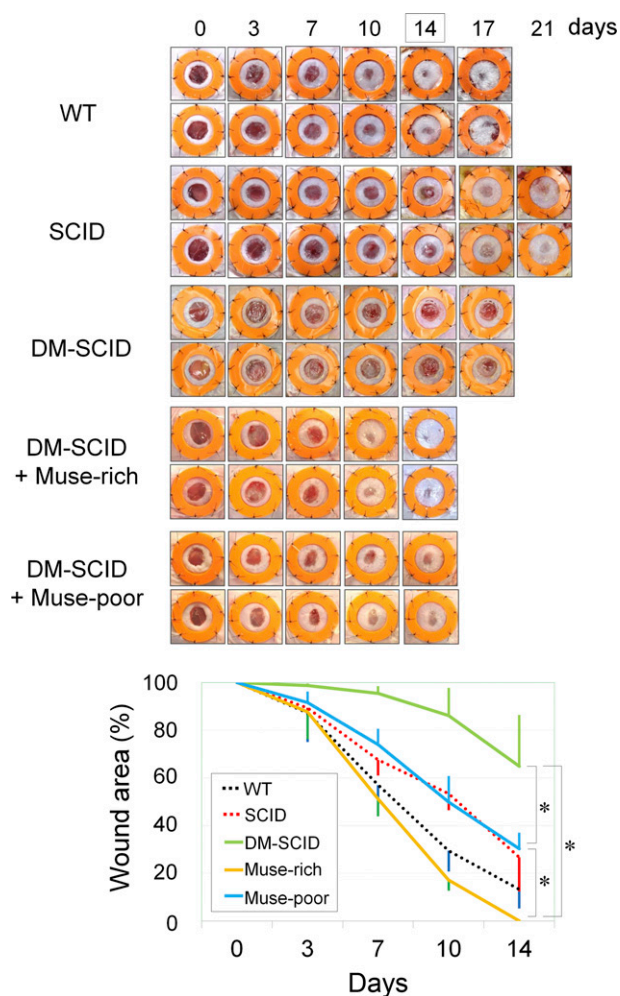

Figure 5. Wound healing of skin ulcers treated with Muse-rich and Muse-poor cell populations. Wound healing of skin defects (6 mm in diameter) was sequentially evaluated for up to 14 days. The wound area was photographed, and the percentage of the wound area to the original wound size was calculated using digital imaging software. Although SCID mice originally showed slightly delayed wound healing compared with their WT counterparts, the wound healing in the STZ-induced DM-SCID mice was more impaired than that in the SCID mice. Wound closure was significantly faster in the DM-SCID mice treated with the Muse-rich cell population than in Muse-poor-treated DM-SCID mice, which showed significantly better wound healing than the nontreated DM-SCID mice. Six mice were used in each group. ∗, $p <$ .05. Abbreviations: DM-SCID, diabetes mellitus-induced SCID mice; Muse, multilineage-differentiating stress-enduring; SCID, severe combined immunodeficiency; STZ, streptozotocin; WT, wild-type.

in the WT group. The effect of the vehicle (hyaluronic acid) used in the cell treatments was also evaluated and showed no significant promoting effects of the vehicle (supplemental online Fig. 2).

Immunohistological Tracing of Transplanted Human Cells

The immunohistologic findings for the human Golgi complex suggested that transplanted human cells were detected in the dermis of the wounded area on day 14 in both Muse-rich and Muse-poor samples. However, the human Golgi complex-positive cells were not observed in the surrounding intact area (Fig. 6). Human Golgi
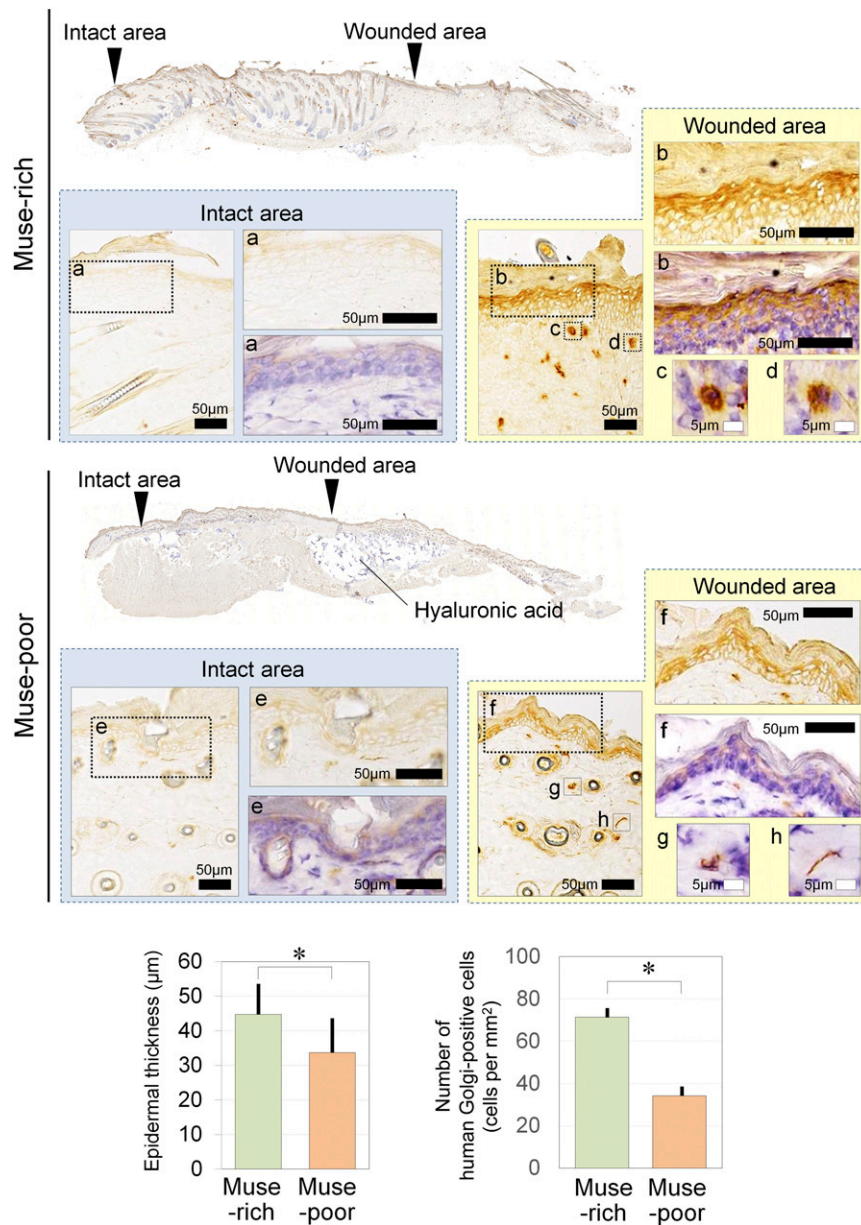
Figure 6.   Immunohistologic findings for human Golgi complex of diabetes mellitus-induced severe combined immunodeficiency wounds treated with Muse-rich or Muse-poor cell populations. Shown are high-magnification views of the intact epidermis (a), repaired epidermis (b), and wounded area (c, d) in Muse-rich sample. Also shown are high-magnification views of the intact epidermis (e), repaired epidermis area (f), and wounded area (g, h) in Muse-poor sample. Human Golgi complex-positive cells, which are equivalent to transplanted human cells, were observed in the epidermis and dermis of the wounded area in both Muse-rich and Muse-poor samples after 14 days. However, human Golgi complex-positive cells were not detected in the surrounding intact area in either group. Transplanted human cells were significantly more frequently detected in Muse-rich samples compared with Muse-poor samples (p = .0006). A significantly thicker epidermis was also noted in Muse-rich samples (p = .0053). ∗, $p < .05$. Abbreviation: Muse, multilineage-differentiating stress-enduring.

complex-positive cells were detected in the Muse-rich samples at significantly larger numbers compared with the Muse-poor samples (Muse-rich, 71.4 $\pm$ 4.6 cells per mm^2; Muse-poor, 34.2 $\pm$ 4.6 cells per mm^2; p = .0006). A significantly thicker epidermis was also noted in the Muse-rich samples (p = .0053). Injected hyaluronic acid deposits were generally recognized in the subcutaneous layer. The cells positive for human Golgi complex were also positive for PECAM-1 (Muse-rich, 186.1 $\pm$ 9.8 cells per mm^2; Muse-poor, 156.7 $\pm$ 13.9 cells per mm^2; p = .144). In contrast, many Golgi complex-positive cells in the middle to lower dermis

were not positive for human PECAM-1 or isolectin in the Muse-rich samples at day 14 (Fig. 7). The number of PECAM-1-positive vascular endothelial cells was comparable between the Muse-rich and Muse-poor samples (Muse-rich, 186.1 $\pm$ 9.8 cells per mm^2; Muse-poor, 156.7 $\pm$ 13.9 cells per mm^2; p = .144), although the ratio of human-derived cells in the PECAM-1-positive cells was higher in the Muse-rich samples (Muse-rich, 22.8% $\pm$ 3.2%; Muse-poor, 12.5% $\pm$ 1.1%; p = .02). These data suggest that transplanted Muse cells survived in the dermis and have differentiated into vascular endothelial cells or other cell types.
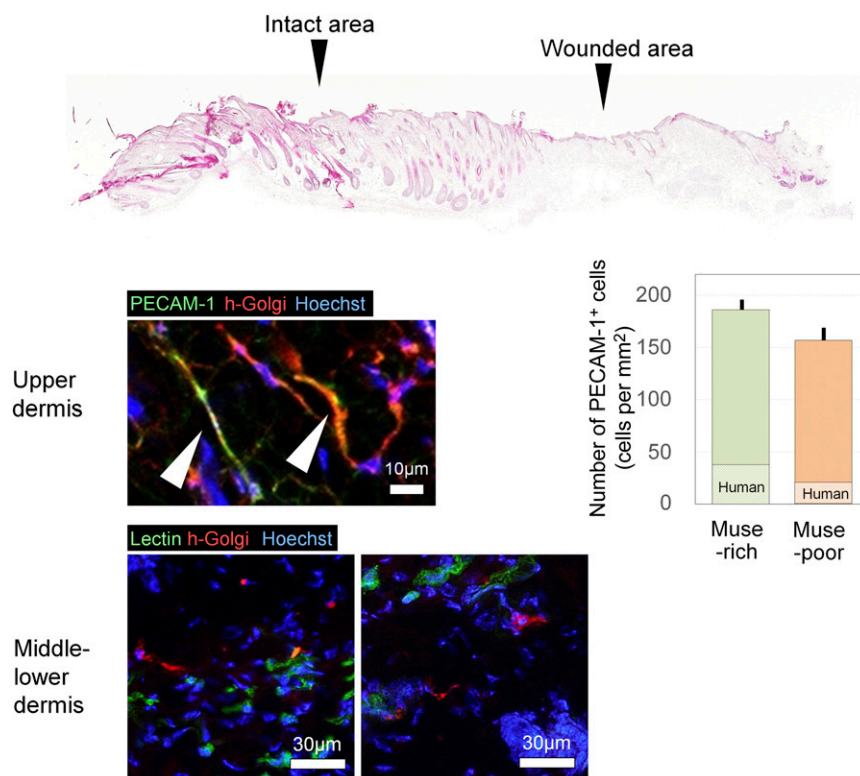
Figure 7. Immunohistologic findings of differentiation markers expressed by transplanted Muse-rich cells. Double immunohistochemistry was performed for human-specific proteins (human Golgi complex) and differentiation markers (PECAM-1 or isolectin) to characterize transplanted Muse-rich cells at day 14. Some cells expressing human Golgi complex were positive for PECAM-1 or isolectin, suggesting differentiation into vascular endothelial cells in the upper dermis; however, human Golgi complex-positive cells in the middle and lower dermis were negative for PECAM-1 and isolectin. The number of PECAM-1$^+$ cells per microscopic field was counted, with no significant difference between the two groups ($p = .144$), although the ratio of human-derived cells was higher in the Muse-rich samples ($p = .02$). Abbreviations: h-Golgi, human Golgi complex; Muse, multilineage-differentiating stress-enduring; PECAM-1, platelet endothelial cell adhesion molecule-1.

DISCUSSION

In the present study, we used a single pluripotent stem cell marker, SSEA-3, for Muse cell isolation and purification. Previous reports have investigated Muse cells derived from human adipose tissue (previously termed "adipose Muse" [10], "Muse-AT" [9], or, in our study, Muse ASCs), which were shown to also be positive for CD105 and to differentiate into cells representative of the three germ layers from a single cell [10]. In addition, Muse cells could be efficiently isolated as cells single positive for SSEA-3 in human dermal fibroblasts, because nearly all dermal fibroblasts were positive for CD105 [6, 12]. Although fluorescence activated cell sorting (FACS) or stress conditions were used in previous studies [6, 9, 12, 18, 19], we used autoMACS, with double collection of the positive fraction after preliminary optimization experiments. MACS purification of Muse cells was not perfect (less than 90%). However, MACS appears to be the most practical method to purify Muse cells, because it is a clinically approved cell separation method and enabled higher Muse purification than other isolations using FACS or stress application. Although Muse cells were initially identified as stress-tolerant cells [6], selection using SSEA-3 collected the same Muse population [10, 12]. Because it remains challenging to efficiently expand the number of Muse cells, we used regular adherent cell culture with hundreds of culture dishes to achieve sufficient numbers of Muse cells for the animal experiments.

We confirmed the superiority of Muse cells compared with non-Muse MSCs (i.e., nearly equal to general ASCs in the present study) in promoting wound healing in diabetic mice, which have impaired healing of skin defects. Ulcers treated with Muse-rich cells healed faster with a thicker epidermis than those treated with Muse-poor cells, with the duration of wound closure even shorter than that in WT mice. In order to test the therapeutic value of human Muse cells for diabetic ulcers, we prepared a diabetic immunodeficient mice model by inducing DM in SCID mice using STZ injections. This mouse model showed impaired wound healing. Our protocol of STZ injection induced DM in SCID mice with a consistent success rate of approximately 75%. Hyperglycemia was well maintained, even 1 year after induction (data not shown). Although systemic administration procedures (e.g., intravenous injection) of Muse cells were reported previously [6, 8], we used local injection of Muse cells with hyaluronic acid as the carrier to treat localized skin wounds to avoid unfavorable cell migration and achieve better concentrated treatment effects. The injections were histologically confirmed and localized in the subcutis around the wound. Hyaluronic acid has been used as a preferable carrier or scaffold, although the appropriate state (cross-linked or non-cross-linked) and concentration are controversial and should be optimized in future studies [20–22].

The mechanism of the wound healing-promoting effects of Muse cells remains to be elucidated. Although Muse-poor ASCs also promoted wound healing in DM-SCID mice, the Muse cells

in the ASC populations showed a higher power to accelerate tissue repair, suggesting that SSEA-3$^+$ Muse ASCs are a selected ASC population with distinct therapeutic potential. Our histological assays showed that Muse-rich ASCs were integrated into the repaired dermis. Some of the injected cells were detected as vascular endothelial cells and as other cells in the upper and lower dermis, respectively. Although the proliferative capacity of Muse cells is not that great, they were previously mentioned as pluripotent stem cells but are nontumorigenic and might be a potent tool for clinical use [6, 9, 10, 18], which was partly supported our findings.

In addition, ASCs have been reported to home to damaged regions and secrete the growth factors required for the inflammatory and proliferating phases of wound healing, such as PDGF, bFGF, TGF-β, and EGF [23]. Microarray assays in our study showed that the expression of growth factors, including PDGF-A, EGF, and SDF-1, was upregulated in Muse-rich cells cultured under hyperoxic conditions (20% O_2), although a limitation existed in that the array used only one sample from each group. In addition, upregulation of pluripotent markers, such as NANOG, suggest a high differentiation potential for Muse cells. Our ELISA results also indicated that Muse cells secrete several growth factors, including PDGF-BB, TGF-β, bFGF, and TNF-α, in larger amounts than in non-Muse cells, particularly under hypoxic (1% O_2) conditions compared with normoxic (6% O_2) conditions. PDGF-BB, TGF-β, and bFGF are known to be involved in the initial coagulating phase of wound healing to promote a series of subsequent events [24]. In contrast, TNF-α is released during the acute inflammatory phase and triggers the inflammatory cascade [25, 26]. TNF-α null mice showed delayed epithelialization in dorsal full-thickness skin defects, suggesting that TNF-α is essential for wound healing [27]. These data collectively suggest that Muse cells might function better under stressful conditions (e.g., hypoxia) and coordinate cellular events in the wound healing process by releasing soluble factors. The diabetic skin ulcers used in the present study are generally refractory to healing, with ischemia and chronic inflammation present, and appear to be a reasonable therapeutic target of Muse cells.

CONCLUSION

In the present study, a selected population of ASCs, namely Muse cells, was shown to have greater therapeutic effects in accelerating the impaired wound healing associated with type 1 DM. On the basis of the suspected mechanisms, our data further suggest their clinical potential in a variety of stem cell-depleted or ischemic conditions of any organ or tissue. Adipose tissue has been gaining more attention as a practical source of adult stem cells. The therapeutic potentials of ASCs were suggested for treating various DM conditions, such as hyperglycemia [28] and autoimmune DM [29]. ASCs were shown to share most biological characteristics, and to have comparable functions, with bone marrow-derived MSCs. Recent studies have suggested that ASCs (and also other tissue-resident MSCs) can be supplied from the bone marrow as tissue-localized stem/progenitor cells [30, 31]. Bone marrow is the central factory and bank of stem/progenitor cells, which are mobilized and delivered on demand by peripheral organs. These data suggest that invasive damage to the bone marrow while harvesting bone marrow-derived cells might have been underestimated. ASCs can be obtained in much larger quantities using minimally invasive approaches that will not damage the bone marrow, suggesting a clinical potential for Muse ASCs in the future.

AUTHOR CONTRIBUTIONS

K. Kinoshita: conception and design, collection and/or assembly of data, data analysis and interpretation, manuscript writing; S.K., H.I., and N.A.: collection and/or assembly of data, data analysis and interpretation; K.M., H.K., K.D., K. Kanayama, J.F., and T.M.: collection and/or assembly of data; A.K.: data analysis and interpretation; K.Y.: conception and design, data analysis and interpretation, financial support, administrative support, final approval of manuscript, manuscript writing.

DISCLOSURE OF POTENTIAL CONFLICTS OF INTEREST

The authors indicated no potential conflicts of interest.

REFERENCES

1 Petersen BE, Bowen WC, Patrene KD et al. Bone marrow as a potential source of hepatic oval cells. Science 1999;284:1168–1170.
2 Harris RG, Herzog EL, Bruscia EM et al. Lack of a fusion requirement for development of bone marrow-derived epithelia. Science 2004;305:90–93.
3 Ren G, Chen X, Dong F et al. Concise review: Mesenchymal stem cells and translational medicine: Emerging issues. STEM CELLS TRANSLATIONAL MEDICINE 2012;1:51–58.
4 Amoh Y, Li L, Katsuoka K et al. Multipotent nestin-positive, keratin-negative hair-follicle bulge stem cells can form neurons. Proc Natl Acad Sci USA 2005;102:5530–5534.

5 Toma JG, Akhavan M, Fernandes KJ et al. Isolation of multipotent adult stem cells from the dermis of mammalian skin. Nat Cell Biol 2001;3:778–784.
6 Kuroda Y, Kitada M, Wakao S et al. Unique multipotent cells in adult human mesenchymal cell populations. Proc Natl Acad Sci USA 2010;107:8639–8643.
7 Yang Z, Liu J, Liu H et al. Isolation and characterization of SSEA3(+) stem cells derived from goat skin fibroblasts. Cell Reprogram 2013;15:195–205.
8 Wakao S, Kitada M, Kuroda Y et al. Multilineage-differentiating stress-enduring (Muse) cells are a primary source of induced pluripotent stem cells in human fibroblasts. Proc Natl Acad Sci USA 2011;108:9875–9880.

9 Heneidi S, Simerman AA, Keller E et al. Awakened by cellular stress: Isolation and characterization of a novel population of pluripotent stem cells derived from human adipose tissue. PLoS One 2013;8:e64752.
10 Ogura F, Wakao S, Kuroda Y et al. Human adipose tissue possesses a unique population of pluripotent stem cells with nontumorigenic and low telomerase activities: Potential implications in regenerative medicine. Stem Cells Dev 2014;23:717–728.
11 Yoshimura K, Shigeura T, Matsumoto D et al. Characterization of freshly isolated and cultured cells derived from the fatty and fluid portions of liposuction aspirates. J Cell Physiol 2006;208:64–76.

12 Tsuchiyama K, Wakao S, Kuroda Y et al. Functional melanocytes are readily reprogrammable from multilineage-differentiating stress-enduring (muse) cells, distinct stem cells in human fibroblasts. J Invest Dermatol 2013; 133:2425–2435.

13 Galiano RD, Michaels J V., Dobryansky M et al. Quantitative and reproducible murine model of excisional wound healing. Wound Repair Regen 2004;12:485–492.

14 Tepper OM, Carr J, Allen RJ Jr et al. Decreased circulating progenitor cell number and failed mechanisms of stromal cell-derived factor-1alpha mediated bone marrow mobilization impair diabetic tissue repair. Diabetes 2010;59:1974–1983.

15 Schmidt RE, Dorsey DA, Beaudet LN et al. Non-obese diabetic mice rapidly develop dramatic sympathetic neuritic dystrophy: A new experimental model of diabetic autonomic neuropathy. Am J Pathol 2003;163: 2077–2091.

16 Lee RH, Seo MJ, Reger RL et al. Multipotent stromal cells from human marrow home to and promote repair of pancreatic islets and renal glomeruli in diabetic NOD/SCID mice. Proc Natl Acad Sci USA 2006;103:17438–17443.

17 Schmidt RE, Green KG, Feng D et al. Erythropoietin and its carbamylated derivative prevent the development of experimental diabetic autonomic neuropathy in STZ-induced diabetic NOD-SCID mice. Exp Neurol 2008; 209:161–170.

18 Wakao S, Akashi H, Kushida Y et al. Muse cells, newly found non-tumorigenic pluripotent stem cells, reside in human mesenchymal tissues. Pathol Int 2014;64:1–9.

19 Kuroda Y, Wakao S, Kitada M et al. Isolation, culture and evaluation of multilineage-differentiating stress-enduring (Muse) cells. Nat Protoc 2013;8:1391–1415.

20 Kablik J, Monheit GD, Yu L et al. Comparative physical properties of hyaluronic acid dermal fillers. Dermatol Surg 2009;35(suppl 1):302–312.

21 Itoi Y, Takatori M, Hyakusoku H et al. Comparison of readily available scaffolds for adipose tissue engineering using adipose-derived stem cells. J Plast Reconstr Aesthet Surg 2010; 63:858–864.

22 Açil Y, Zhang X, Nitsche T et al. Effects of different scaffolds on rat adipose tissue derived stroma cells. J Craniomaxillofac Surg 2014;42: 825–834.

23 Maxson S, Lopez EA, Yoo D et al. Concise review: Role of mesenchymal stem cells in wound repair. Stem Cells Translational Medicine 2012;1:142–149.

24 Eto H, Suga H, Inoueoi K et al. Adipose injury-associated factors mitigate hypoxia in ischemic tissues through activation of adipose stem/stromal cells and induction angiogenesis. Am J Pathol 2011;178:2322–2332.

25 Mooney DP, O'Reilly M, Gamelli RL. Tumor necrosis factor and wound healing. Ann Surg 1990;211:124–129.

26 Salomon GD, Kasid A, Cromack DT et al. The local effects of cachectin/tumor necrosis factor on wound healing. Ann Surg 1991;214: 175–180.

27 Shinozaki M, Okada Y, Kitano A et al. Impaired cutaneous wound healing with excess granulation tissue formation in TNFalpha-null mice. Arch Dermatol Res 2009;301:531–537.

28 Kono TM, Sims EK, Moss DR et al. Human adipose-derived stromal/stem cells protect against STZ-induced hyperglycemia: Analysis of hASC-derived paracrine effectors. Stem Cells 2014;32:1831–1842.

29 Bassi ÊJ, Moraes-Vieira PM, Moreira-Sá CS et al. Immune regulatory properties of allogeneic adipose-derived mesenchymal stem cells in the treatment of experimental autoimmune diabetes. Diabetes 2012;61:2534–2545.

30 Hausman GJ, Hausman DB. Search for the preadipocyte progenitor cell. J Clin Invest 2006; 116:3103–3106.

31 Eto H, Ishimine H, Kinoshita K et al. Characterization of human adipose tissue-resident hematopoietic cell populations reveals a novel macrophage subpopulation with CD34 expression and mesenchymal multipotency. Stem Cells Dev 2013;22:985–997.

See www.StemCellsTM.com for supporting information available online.